BIOCHEMISTRY
including biophysical chemistry & molecular biology

Accelerated Publication

pubs.acs.org/biochemistry

Full-Length Human Glutaminase in Complex with an Allosteric Inhibitor

Byron DeLaBarre,*[,†] Stefan Gross,[†] Cheng Fang,[§] Yi Gao,[§] Abhishek Jha,[†] Fan Jiang,[‡] Juanhua Song J.,[‡] Wentao Wei,[‡] and Jonathan B. Hurov[†]

[†]Agios Pharmaceuticals, 38 Sidney Street, 2nd Floor, Cambridge, Massachusetts 02139-4169, United States

[‡]Viva Biotech, 334 Aidisheng Road, Zhangjiang High-tech Park Pudong New Area, Shanghai, China

[§]ChemPartner, No. 5 Building, 998 Halei Road, Zhangjiang Hi-tech Park Pudong New Area, Shanghai, China

Supporting Information

ABSTRACT: Glutaminase (GLS1/2) catalyzes the conversion of L-glutamine to L-glutamate and ammonia. The level of a splice variant of GLS1 (GAC) is elevated in certain cancers, and GAC is specifically inhibited by bis-2-(5-phenylacetimido-1,2,4,thiadiazol-2-yl)ethyl sulfide (BPTES). We report here the first full-length crystal structure of GAC in the presence and absence of BPTES molecules. Two BPTES molecules bind at an interface region of the GAC tetramer in a manner that appears to lock the GAC tetramer into a nonproductive conformation. The importance of these loops with regard to overall enzymatic activity of the tetramer was revealed by a series of GAC point mutants designed to create a BPTES resistant GAC.

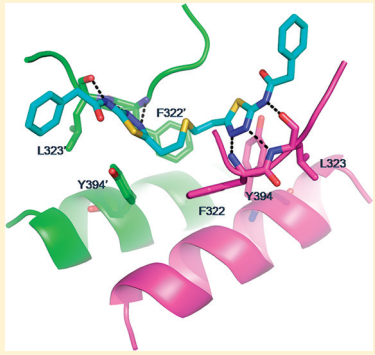

Glutamine is the most abundant amino acid in the blood and is an essential nutrient for highly proliferative cells such as those found in tumors.[1−3] When glutamine is taken up by the cell, a significant fraction of it is converted to glutamate and ammonia by glutaminase (GLS) in the mitochondria. Glutamate can be oxidized to α-ketoglutarate to feed the TCA cycle or be used for the biosynthesis of several other amino acids and lipids. In this manner, glutamine can fulfill both the energetic and biomass requirements of proliferating cells.

In addition to the role of glutaminase in anaplerotic processes, several other biological functions have been attributed to glutaminase activity.[4] In humans, there are two distinct genes encoding glutaminase enzymes: GLS1 and GLS2. The GLS1 enzyme is expressed at high levels in kidney and brain tissue. In the kidney, GLS1 is believed to maintain acid−base balance during metabolic acidosis. Renal GLS1 activity in rats is elevated in response to acidosis, and this regulation is at least in part mediated by pH-responsive stabilization of GLS1 mRNA.[5,6] GLS2 is predominantly expressed in the liver where it provides nitrogen for the urea cycle.

In the central nervous system, GLS1 activity is proposed to generate a significant amount of the total neuronal glutamate pool that in turn acts as an excitatory neurotransmitter.[7−9] GLS1 activity may therefore be essential for the optimal function of multiple central nervous system glutamate receptors and their downstream roles in both the normal and pathological brain. GLS1 germline knockout mice die postnatally with impairment of neuronal glutamatergic signal transmission. Heterozygous GLS1 mice exhibit decreased sensitivity to psychotic challenges, consistent with reduced glutamatergic synaptic transmission.[10] In the peripheral nervous system, GLS1 expression and activity in the dorsal root ganglia have been proposed to generate glutamate pools involved in inflammatory pain, suggesting a role for glutaminase inhibitors in the modulation of nociceptor function.[11] Finally, HIV-associated dementia has been linked to upregulation of glutaminase activity and subsequent glutamate excitoxicity derived from HIV-infected macrophages.[12,13]

Multiple GLS1 transcripts have been described: canonical splice variant 1 (KGA), a truncated and noncatalytically competent splice variant 2, and an elongated splice variant 3 (GAC) that is identical to KGA with a variation at the C-terminus. The GAC variant of GLS1 is strongly expressed in many primary tumors and tumor cell lines, while GLS2 expression appears to be relatively limited in cancer.[14] GLS1 expression was shown to be positively regulated by myc and was identified as an important effector of Rho GTPase-mediated transformation.[15,16]

Previous work had identified bis-2-(5-phenylacetimido-1,2,4-thiadiazol-2-yl)ethyl sulfide (BPTES), a compound that selectively inhibits GLS1 versus GLS2 enzymatic activity (Figure 1 and Table 1).[17] Kinetic characterization of the interaction of BPTES with GLS1 revealed a mixed mode inhibition. Biophysical measurements demonstrated that BPTES could affect the dimer−tetramer equilibrium of GLS1. Other factors such as inorganic phosphate and protein concentration can also influence the oligomerization of GLS.

Received: October 23, 2011
Published: November 3, 2011

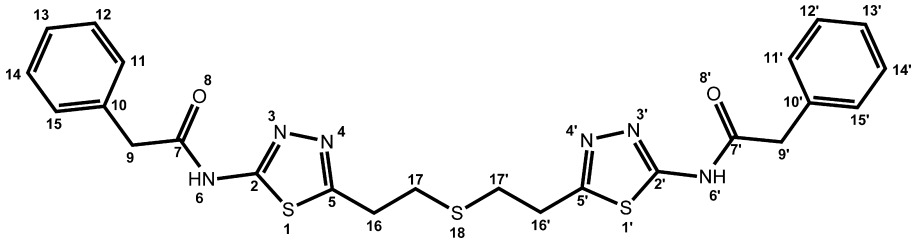

Figure 1. BPTES molecule.

Table 1. Enzymatic Characterization of Glutaminase Isoforms and BPTES Resistant Mutants

enzyme	k_{cat} (s^{-1})	K_M(glutamine) mM	k_{cat}/K_M (M^{-1} s^{-1})	K_a(phosphate) (mM)	BPTES IC_{50} (μM)
GAC	22 ± 2	1.4 ± 0.4	(1.6 ± 0.5) × 10^4	80 ± 8	0.08 ± 0.02
GLS1	10 ± 1	1.9 ± 0.4	(5.3 ± 1.2) × 10^3	76 ± 7	0.06 ± 0.06
GLS2	2.5 ± 0.3	4.0 ± 0.2	(6.3 ± 0.8) × 10^2	8 ± 1	88 ± 17
GAC F322S/F318Y	40 ± 1.5	2.5 ± 0.1	(1.6 ± 0.1) × 10^4	4 ± 2	>100
GAC Y394L	20 ± 1	0.4 ± 0.1	(4.7 ± 1.2) × 10^4	59 ± 19	>100

However, the BPTES-induced GLS1 tetramer migrates at Svedberg values different from those observed for the phosphate-induced tetramer of GLS1. The Svedberg differential implies that BPTES induces a tetramer with a conformation that is different from that of the phosphate-activated tetramer. Taken together, the data were suggestive of an allosteric inhibition by BPTES in a manner that alters the tetramer conformation.

To improve our understanding of the mechanism of glutaminase inhibition by BPTES, we crystallized and determined the structure of full-length human GAC both with and without BPTES bound to the molecule. We then created GAC mutants based upon observed interactions between BPTES and its binding pocket in GAC and sequence differences in the BPTES binding pocket among GLS1, GLS2, and a bacterial form of GLS1. The mutants exhibited essentially wild-type GAC activity but were insensitive to inhibition by the BPTES molecule. Interestingly, the mutants also conveyed the phosphate activation behavior of GLS2 into GLS1, despite being remote from the phosphate binding site. The BPTES resistant mutants provide insight into the differential activity of BPTES on GLS1 versus GLS2, aid in improving our understanding of the implications of the two new protein crystal structures, and can serve as "tool proteins" for measuring potential off target effects of BPTES and BPTES-related molecules.

MATERIALS AND METHODS

Cloning, Expression, and Purification of GAC Mutants for Enzymology Studies. The cDNA of GAC (GAC, AF158555) was purchased from Genecopeia in the pDONR vector. The coding region was amplified from an open reading frame in a pDONR vector by polymerase chain reaction using primers designed to add XbaI and HindIII restrictions sites at the 5′ and 3′ ends, respectively, and an extra sequence encoding a C-terminal six-His tag was added at the 3′ end to facilitate protein purification. The resultant fragment was cloned into vector pFastBac1 (Invitrogen). Site-directed mutagenesis was performed on the pFastBac1-GAC plasmid using the QuikChange Lightning Site-Directed Mutagenesis Kit (Stratagene) to create the GLS1 mutants described herein. The cDNA of human glutaminase 1 (GLS1; NM_014905.2) was purchased from OriGene in the pCMV6-XL4 vector, and the cDNA of GLS2 in the pENTR223.1 vector (GLS2, BC166649) was purchased from Open Biosystems. They were both similarly amplified for subcloning into pFastBac1.

pFastBac1-GAC and pFastBac1-GLS2 were transformed into DH10Bac *Escherichia coli* for transposition into bacmid, and positive clones were selected on a blue/white LB agar plate. Recombinant bacmid was isolated from positive clones with the PureLink Hipure Plasmid DNA miniprep kit (Invitrogen) and transfected into SF9 cells (Invitrogen) to generate recombinant virus stocks, which were amplified for two cycles before infection of SF9 cells at a multiplicity of infection (MOI) of 2. Infected cells were harvested 96 h postinfection and resuspended in lysis buffer [50 mM KH_2PO_4 (pH 7.5), 300 mM NaCl, 10 mM imidazole, 10% glycerol, and 1 mM PMSF] and disrupted by microfluidization. The cell lysate was clarified by centrifugation at 20000*g* for 60 min before being loaded on a metal chelate affinity resin equilibrated with nickel column buffer A [50 mM KH_2PO_4 (pH 7.5), 300 mM NaCl, 10 mM imidazole, and 10% glycerol] and washed via a 20 column volume linear gradient from 10 to 100% nickel column buffer B [50 mM KH_2PO_4 (pH 7.5), 300 mM NaCl, 10 mM imidazole, 500 mM imidazole, and 10% glycerol]. Fractions containing the protein of interest were identified by sodium dodecyl sulfate−polyacrylamide gel electrophoresis (SDS−PAGE), pooled, and buffer exchanged into storage buffer [50 mM Tris (pH 8.0) and 500 mM NaCl] with a G25 column for storage at −80 °C. The 70 N-terminal residues of GAC, comprising the mitochondrial localization sequence, were cleaved at some point during SF9 cell expression. This posttranslational modification was first made evident by a lower observed molecular weight on the SDS−PAGE gels of the expressed and purified protein and subsequently verified by both intact protein mass spectrometry and N-terminal protein sequencing (data not shown).

Preparation of Protein for Crystallography. GAC was expressed in SF9 cells as described above. Cell pellets were resuspended with 25 mM HEPES (pH 7.5), 50 mM NaCl, 5% glycerol, 5 mM β-ME, and 20 mM imidazole with protease inhibitors (buffer C) and stored at −80 °C. Mild sonication was used to lyse thawed cells. Cell debris was removed by centrifugation at 26000*g* for 1 h. The soluble fraction was applied to the Ni-NTA affinity column pre-equilibrated with buffer C. GAC was eluted with elution buffer [25 mM HEPES (pH 7.5), 200 mM NaCl, 5% glycerol, 5 mM β-ME, and 250

mM imidazole] and dialyzed overnight at 4 °C in buffer C. Dialysate was loaded onto a Hi-trap HQ 5 mL column (Amersham Biotech). Bound protein was eluted via one-step elution with 25 mM HEPES (pH 7.5), 200 mM NaCl, 5% glycerol, and 5 mM β-ME. The eluted GAC protein was snap frozen in liquid N_2 for use in the crystallization study.

Preparation of the GAC−BPTES Complex for Crystallization. GAC (0.45 mM), 10 mM bis-2-(5-phenylacetamido-1,2,4-thiadiazol-2-yl)ethyl sulfide (BPTES) (SaiAdvantium, Hyderabad, India), and 10 mM glutamate were mixed and incubated at 18 °C for 2 h. A small amount of precipitate was removed postincubation by centrifugation at 20000*g* for 15 min. The supernatant fraction containing the GAC−BPTES complex was immediately subjected to crystallization trials.

Crystallization, Data Collection, and Structure Determination. Crystals of the GAC−BPTES complex were grown by hanging drop vapor diffusion, by mixing the complex sample with an equal volume of reservoir solution containing 0.3 M magnesium chloride, 0.1 M Tris (pH 8.5), and 12% (w/v) PEG 4000. Crystals appeared overnight and grew to full size within 3−5 days. The crystals of GAC without BPTES were grown under conditions similar to those observed for the GAC−BPTES complex, the only change besides omission of BPTES being a reduction from 300 to 200 mM magnesium chloride. Crystals were equilibrated in a cryoprotectant buffer containing reservoir buffer and 25% (v/v) glycerol and were flash-frozen in a cold nitrogen stream at −170 °C.

GAC crystallized in space group $P2_1$, with the following unit cell parameters: a = 50.660 Å, b = 139.614 Å, c = 178.385 Å, α = 90°, β = 94.14°, and γ = 90°. The GAC−BTPES complex crystallized in space group $P2_1$ with the following unit cell parameters: a = 50.117 Å, b = 139.434 Å, c = 177.713 Å, α = 90°, β = 93.73°, and γ = 90°. There was one GAC tetramer per asymmetric unit for both GAC and the GAC−BPTES complex. A 2.3 Å data set for the GAC−BPTES complex and a 2.6 Å data set for GAC were collected at the Shanghai Synchrotron Radiation Facility. These data sets were integrated and scaled using HKL2000.[18] Statistics for the collected data are summarized in Table 2. The structure was determined by molecular replacement with MOLREP using a molecule comprised of residues 222−532 of human GLS1 (Protein Data Bank entry 3CZD) as a search model. After rigid-body refinement, model building and refinement were performed using COOT (Emsley, 2004) and Refmac from the CCP4 package.[19] The electron density maps from $2F_o - F_c$ and $F_o - F_c$ calculations were sufficient for model building but were substantially improved with the CCP4 program Pirate. Finally, TOP[20] was used to automatically adjust the backbone ϕ and ψ angles of the proteins to produce the final models. R_{work} and R_{free} for the final model of GAC are 23.7 and 27.3%, respectively. R_{work} and R_{free} for the final model of the GAC−BPTES complex are 22.9 and 26.8%, respectively. The Ramachandran plots drawn with PROCHECK[21] shows that 98.1, 1.2, and 0.7% of all residues in GAC and 96, 3.3, and 0.7% of all residues in the GAC−BPTES complex fall within most favored, allowed, and disallowed regions, respectively.

Enzymology of GAC Mutants and Isoforms. GAC enzyme activity was measured in an assay system coupled to glutamate oxidase (GluOx, Sigma) in which the amount of hydrogen peroxide produced by GluOx was measured by reduction of resazurin to resorufin in the presence of horseradish peroxidase (Sigma). The amount of resorufin produced in the enzymatic assays was measured in a SpectraMax plate reader with excitation at 544 nm and emission at 590 nm against a standard curve of resorufin prepared in assay buffer without GAC. Enzyme assays were performed in a buffer containing 50 mM HEPES, 50 mM phosphate, 150 mM NaCl, 0.25 mM EDTA, 0.05% (w/v) BSA, 0.00003 unit/μL glutamate oxidase, 0.1 unit/mL HRP, 20 μM resazurin, and 0.08 μg/mL glutaminase (pH 8.5) at room temperature. Determination of kinetic parameters was performed as described in ref 22.

Table 2. Crystal Data Collection and Refinement Statistics[a]

	GAC	GAC−BPTES
	Data Collection	
space group	$P2_1$	$P2_1$
cell dimensions *a*, *b*, *c* (Å)	50.7, 139.6, 178.4	50.1, 139.4, 177.7
resolution (Å)	30−2.55 (2.64−2.55)	50−2.3 (2.38−2.30)
R_{sym}	0.098 (0.498)	0.109 (0.447)
$I/\sigma I$	13.4 (2.4)	13.3 (2.8)
completeness (%)	99.9 (99.3)	99.9 (99.7)
redundancy	4.3 (4.2)	3.8 (3.6)
	Refinement	
resolution (Å)	30−2.55	45−2.3
no. of reflections	75628	103630
R_{work}/R_{free}	0.237/0.273	0.229/0.268
no. of atoms		
protein	12734	13330
water	179	531
ligands	4 glutamate	4 glutamate + 2 BPTES
B factor (Å^2)		
protein	44.7	33.7
glutamate (A/B/C/D)	63.2/62.8/63.9/68.3	45.4/42.7/46.4/52.8
BPTES (1/2)	–	67.1/70.8
root-mean-square deviation		
bond lengths (Å)	0.02	0.02
bond angles (deg)	1.91	1.99

[a]Values in parentheses are for the highest-resolution shell.

RESULTS

Description of the Full-Length GAC Domain Structure. A full-length structure of GAC has not been described previously. The protein crystallized here was comprised of residues 71−598. It is arranged as a tetramer in the asymmetric unit with both long (~1600 Å^2 buried) and short (~640 Å^2 buried) interfaces (Figure 2). With the exception of slight variations in loops at the short dimer interface, each of the four glutamate-bound monomers exhibits identical conformations. For both the unbound and BPTES-bound structures, glutamate is bound in the active site pocket that was previously defined by interactions with covalently bound substrate analogues such as DON and acivicin.[23,24] Residues 71−135 and 547−598 were not visible in the electron density of either structure. There was weak density leading up to the first assigned residue at the N-terminus, but it was insufficient to make proper sequence assignments. Additionally, residues 315−320 were not ordered in the non-BPTES-bound complex.

The protein folds such that the N-terminus and C-terminus are close to one another. The first consistently visible part of the N-terminus is comprised of residues 137−224. These

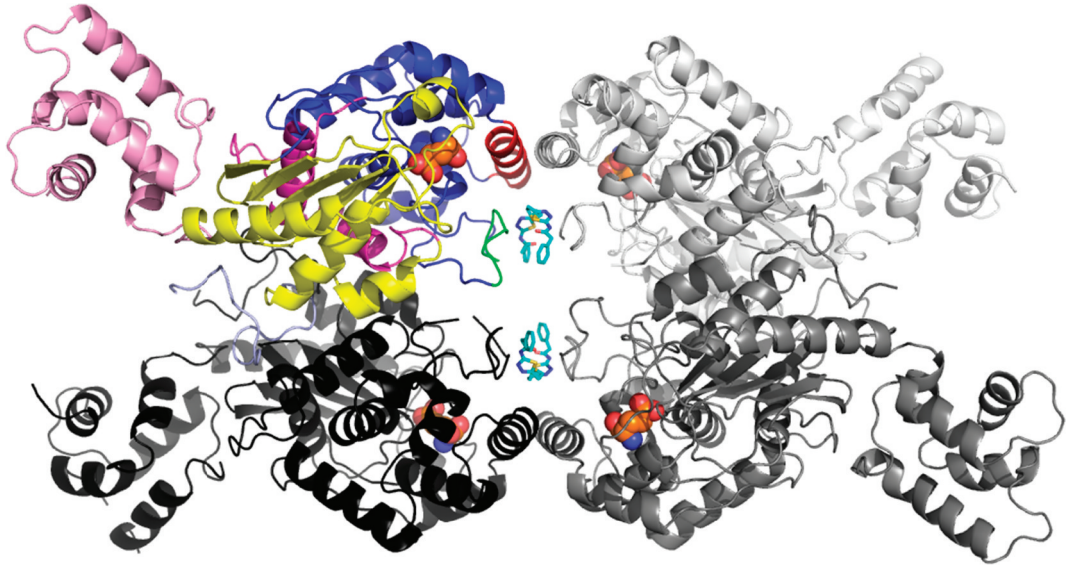

Figure 2. GAC tetramer with BPTES. One monomer has the N-terminal domain colored pink, the α/β domain colored yellow, the extended helical domain colored blue, the short dimer−dimer helix interaction colored red, and the BPTES binding loop colored green. The three remaining tetramers are shown as shades of gray. The BPTES molecule is shown as a cyan stick figure, and the glutamate molecules are shown as orange spheres.

residues form a small helical domain oriented away from any of the tetramer interfaces. Both the N- and C-termini exhibit disorder in this structure, which results in the N-terminal helical domain being flanked by two regions of disordered residues, 71−135 and 547−598.

The N-terminal helical domain is followed by a large α/β domain that is discontinuous in the primary sequence. Residues 224−276, 479−526, and 421−478 comprise an antiparallel β sheet surrounded by several α helices. Two of the α helices, α-16 and α-17 (residues 450−477), comprise most of the long dimer interface.

The α/β domain packs against an extended α helical domain with seven α helices comprised of residues 276−420. This domain contains most of the residues that make up the glutamate binding pocket, a helix (α-13, residues 386−399) that exhibits the most ordered interactions on the short dimer−dimer interface, and the loop (residues 309−334) that provides most of the BPTES binding interactions. The glutamate binding pocket and BPTES binding loops are described in greater detail below. The interfacial helix, α-13, interacts in a head-to-tail fashion with helix α-13 of the adjacent subunit such that Tyr393 from one subunit forms a π-stacking interaction with Phe389 of the other and vice versa. The interaction is further stabilized by salt bridges between Asp386 and Lys396 at both ends of the interface. The extended α helical domain contains the catalytic core of the molecule as well as interactions for stabilizing and potentially communicating the conformation of GAC oligomers.

The α/β domain is followed by a connecting loop (residues 527−546) that leads to the disordered C-terminal splice region. The connecting loop forms several contacts on the long dimer edge with the α/β domain of the neighboring molecule. The remaining disordered residues (547−599), which include the splice variation, are oriented toward the periphery of the tetrameric molecule in approximately the same region as the disordered residues located in the N-terminal portion of the protein.

Glutamate Binding Pocket. The glutamate binding pocket is comprised primarily of residues from the extended helical domain (Figure 3). Asn335 and Tyr414 form hydrogen

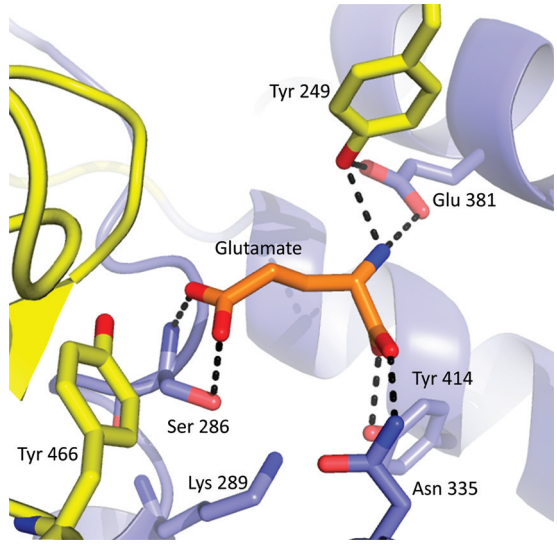

Figure 3. Glutamate binding pocket. Ribbon diagram colored as in Figure 2 with the bound glutmate shown as an orange stick. Key amino acids forming H-bonds (except Tyr466 and Lys289) are shown as sticks.

bonds with the α-carboxylate of the bound glutamate, and Glu381 and Tyr249 form hydrogen bonds with the α-amino group of the bound glutamate. Tyr249 is located on an extended loop originating from the central α/β domain. The location of this residue suggests that it may serve as a general acid during the catalytic cycle. The γ-carboxylate of the bound glutamate forms a hydrogen bond with the side chain hydroxyl of Ser286 as well as its backbone amide. Ser286 is covalently modified upon incubation with inhibitors bearing reactive groups. There is a long and presumably weak hydrogen bond

dx.doi.org/10.1021/bi201613d | *Biochemistry* 2011, 50, 10764−10770

between the γ-carboxylate of the bound glutamate and Tyr466 of the α/β domain.

BPTES Binding Location. The BPTES molecule binds at the short dimer−dimer interface where it interacts with the loop region comprised of residues 320−327 and interface helix α-13, residues 386−399 (Figure 4). The interaction occurs in a highly symmetrical fashion with residues from two GLS1 monomers. The BPTES molecule binds at both available interfaces, such that there is one BPTES molecule per GLS1 dimer. The 320−327 loop regions undergo a large rearrangement upon BPTES binding. Phe322 swings into the pocket to combine with Tyr394 to form a hydrophobic "π-basket" that accommodates the central thioether portion of the BPTES molecule. At the same time, Leu321 folds down on top of BPTES, essentially encapsulating the central thioether region of BPTES. The thiadiazolyl amide portion of BPTES forms a series of hydrogen bonds with the BPTES binding loop backbone atoms. $N_{4/4}'$ of the thiadiazole ring forms a poorly aligned hydrogen bond with the backbone amide nitrogen of Phe322, while $N_{3/3}'$ of the thiadiazol and the $N_{6/6}'$ amide nitrogen of BPTES form a favorable pair of hydrogen bonds with the Leu 323 backbone amide nitrogen and carbonyl oxygen atoms, respectively. Electron density was poor to nonexistent for the terminal phenyl rings of the BPTES molecule (Figure 1 of the Supporting Information). This suggests mobility at the termini of the BPTES molecule that extends out into the solvent region.

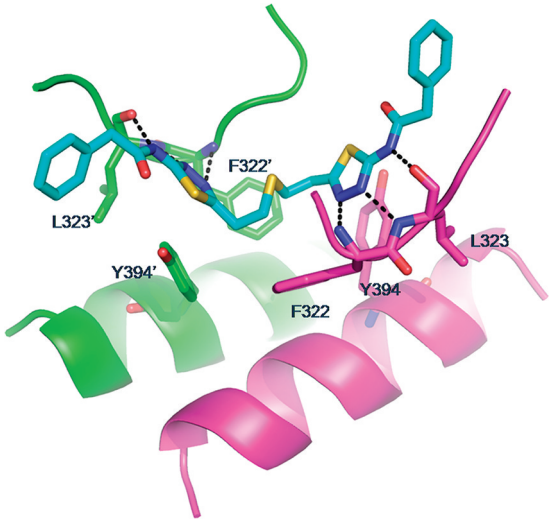

Figure 4. BPTES binding pocket interactions. The BPTES molecule is rendered as a stick and colored by atom type, with cyan carbons, yellow sulfurs, blue nitrogens, and red oxygens. The short dimer interface helices and BPTES binding loops are shown with monomers colored green and maroon. Key hydrogen bond interactions to peptide backbone atoms are represented as dashed lines, and the residues contributing to the hydrophobic π-basket (Y394 and F322) are shown.

BPTES Resistant GLS1Mutants. We sought to evaluate the binding observed in the structure by creating a BPTES resistant mutant that simultaneously showed enzyme kinetics and phosphate activation similar to those of wild-type GAC. Taking into account the observation that GLS2 is resistant to BPTES, we focused our efforts on transferring differences from the GLS2 sequence to GAC in the region of BPTES binding. There are only two differences in the sequences of GAC and GLS2 in the binding pocket (Figure 5): GAC Phe318 aligns with GLS2 Tyr251, and GAC Phe322 aligns with GLS2 Ser255. We also looked to the alignment against bacterial species and found that Tyr394 aligns with Leu174 in the *E. coli* GLSA-2 sequence. Two different mutant forms of GAC were created on the basis of these observations: an F318Y/F322S double mutant and a Y394L single mutant. Both mutants exhibited essentially wild-type kinetics for glutamine binding. For phosphate activation, the mutants exhibited elevated activity at <75 mM phosphate but at higher phosphate concentrations exhibit essentially wild-type behavior (Table 1). Neither mutant protein was significantly inhibited by BPTES (IC_{50} > 100 μM), compared to the IC_{50} of 80 nM observed for wild-type GAC. This represents a >1000-fold decrease in potency for BPTES with respect to the mutant GAC proteins.

DISCUSSION

This work describes the first full-length structure of a human glutaminase enzyme. The structure was determined in the presence and absence of BPTES, a GLS1 selective inhibitor. There are several interesting observations that can be made from this pair of structures.

First, the least ordered regions of the GAC structure as determined here are the extreme N- and C-termini. The C-terminal disordered region is exactly where the splice variation occurs that defines GAC from the canonical GLS1 protein. These two regions of disorder are relatively close in space to one another. Both of these are located near the N-terminal α helical domain, which itself does not appear to be affecting the tetramer interface interactions or the substrate binding pocket. The splice variation at the C-terminus appears to differentiate tissue distribution for GAC versus the canonical form of the enzyme.[14] Furthermore, the second splice variant of GLS1 is comprised of only the N-terminal domain, which suggests that

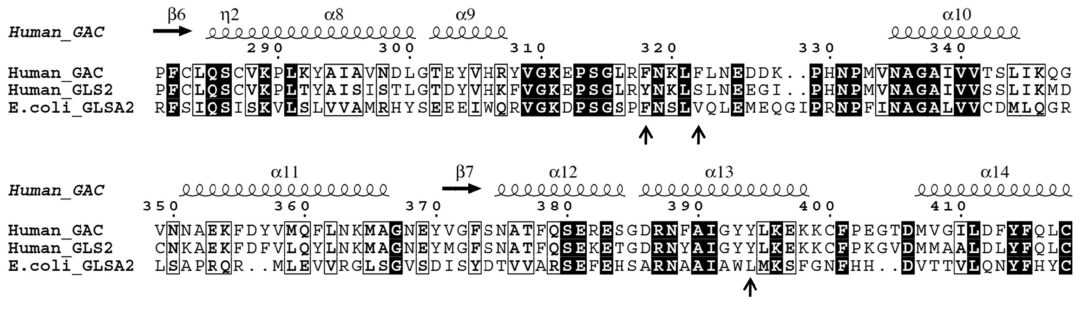

Figure 5. Primary sequence alignment of human GAC, human GLS2, and *E. coli* GLSA2 with structural elements from GAC . Mutation sites for creation of BPTES resistant GAC are denoted with arrows.

dx.doi.org/10.1021/bi201613d | *Biochemistry* 2011, 50, 10764−10770

it may play a role in moderating protein−protein interactions in the context of larger protein complexes. Taken together, these observations suggest that this region of GAC may function as a protein−protein interaction motif. Such an interaction may serve to localize GAC to specific subcellular regions or to bind the glutaminase tetramer within a larger complex associated with its role in metabolism.

Second, the molecule crystallized as a complete tetramer in the asymmetric unit. While the tetramer is the more active oligomeric state of the molecule, the active conformation of the tetramer is not clear. The conformation described here is unlikely to be the catalytically active form of the enzyme. In both of these structures, like most other glutaminase structures,[24] there is a glutamate molecule in the active site of each of the four constituent protomers. The glutaminase structures bound with glutamate, including the one described here, likely represent the enzyme−product complex that occurs following release of ammonia from the active site. Furthermore, in considering what types of residues would be necessary to catalyze the conversion of glutamine to glutamate, there are none within a feasible distance of the glutamate molecule. Several possible residues are close, such as Tyr466 and the Lys289/Ser286 combination, either of which could serve as a general acid to protonate the γ-amino nitrogen of glutamine. There are no structures with a water molecule in the active site, but presumably, the water would be activated by a general base. There are several candidates for this role as well, but none that appear close enough to catalyze a hydrolysis in the current conformation. Finally, there are no conformational changes in the active site between the BPTES-bound and the non-BPTES-bound forms. The significant change observed in residues 315−320 of the loop regions upon BPTES binding provides evidence that movement within the tetramer as crystallized is possible. However, the similarity of the tetramer conformation observed here in the presence and absence of BPTES, along with the slight increase in order reflected by the higher resolution of the BPTES-bound structure, suggests that the glutamate-bound GAC structure observed here represents an inactive conformation of the tetramer. Furthermore, other glutaminase crystal structures show a high degree of similarity to the conformation observed here, suggesting that they too present an inactive form of the enzyme. As the glutaminase reaction has not been described as highly cooperative in steady state enzymatic studies, it seems probable that the actual conformational flexibility of the molecule is complex. In any case, it is difficult to describe the effect of BPTES on the conformation of the catalytic site because no changes outside of the above-mentioned loops are observed with the currently available crystal structures. It is probable that BPTES serves to stabilize the glutamate-bound conformation of the tetramer. The previously described enzyme kinetics for BPTES indicated mixed mode inhibition but showed some aspects of substrate competitive behavior. Sufficient concentrations of glutamine can compete with the bound glutamate, pushing the tetramer into a conformation that is incompatible with BPTES binding. Such a mechanism would be in accord with what is observed in the crystal structures described here.

The loop regions of residues 315−320 that form part of the short dimer interface and are critical to the binding of the BPTES molecule appear to mediate the putative conformational change between the substrate- and product-bound forms. Glutaminase is activated by the presence of phosphate, but GLS1 and GLS2 behave slightly differently from one another. The phosphate binding site is at the N-terminus of helix 12 (residues 375−384) near the active site binding pocket. The observation that it was possible to confer the phosphate activation profile of GLS2 into GLS1 with the transfer of two residues from GLS2 to GLS1 in the BPTES binding loop region suggests that these interface loops play an important role in communicating conformational changes across the entire tetramer. Furthermore, mutations that should have been accommodated by flexible noninteracting loops resulted in proteins that had lost most of their enzymatic activity (data not shown).

We speculate that the allosteric effect of BPTES is to freeze the interface loops that would be used to transmit conformational change throughout the tetramer. This contrasts with other glutaminase inhibitors such as DON and acivicin that were demonstrated to covalently modify the Ser286 residue located in the substrate binding pocket. These compounds have significant toxicity issues. The identification of the new allosteric inhibitory site occupied by the BPTES molecule in the GAC tetramer represents a new opportunity to inhibit GLS1 in a specific manner, potentially avoiding the toxicity observed with other glutaminase inhibitors. As such, the work described here represents a tremendous starting point for the development of drugs based upon the disruption of the cellular metabolism of glutamine.

■ ASSOCIATED CONTENT

Ⓢ Supporting Information

Electron density around BPTES. This material is available free of charge via the Internet at http://pubs.acs.org.

Accession Codes

Coordinates and structure factors have been deposited in the Protein Data Bank as entries 3UNW and 3UO9 .

■ AUTHOR INFORMATION

Corresponding Author

*E-mail: byron.delabarre@agios.com. Phone: (617) 649-8600.

Funding

This work was fully funded by Agios Pharmaceuticals.

Notes

The following authors are employees of and have a financial stake in Agios Pharmaceuticals: B. DeLaBarre, S. Gross, A. Jha, and J. Hurov.

■ ACKNOWLEDGMENTS

We thank Lenny Dang, Rene Lemieux, Lew Cantley, Scott Biller, and Michael Su for a critical reading of the manuscript, discussions, and helpful suggestions regarding the presentation of the work. We thank Zheng Xu for his efforts in coordinating certain aspects of the experimental work. We thank Frank Salituro and Jeremy Travins for oversight of the synthesis of the BPTES molecule. We thank Valeria Fantin for encouraging us to publish the work described here.

■ REFERENCES

(1) Newsholme, E. A., Crabtree, B., and Ardawi, M. S. (1985) Glutamine metabolism in lymphocytes: Its biochemical, physiological and clinical importance. *Exp. Physiol. 70*, 473−489.

(2) Szeliga, M., and Obara-Michlewska, M. (2009) Glutamine in neoplastic cells: Focus on the expression and roles of glutaminases. *Neurochem. Int. 55*, 71−75.

(3) DeBerardinis, R. J., and Cheng, T. (2010) Q's next: The diverse functions of glutamine in metabolism, cell biology and cancer. *Oncogene 29*, 313−324.
(4) Mates, J. M., Segura, J. A., Campos-Sandoval, J. A., Lobo, C., Alonso, L., Alonso, F. J., and Marquez, J. (2009) Glutamine homeostasis and mitochondrial dynamics. *Int. J. Biochem. Cell Biol. 41*, 2051−2061.
(5) Curthoys, N. P. (2001) Role of mitochondrial glutaminase in rat renal glutamine metabolism. *J. Nutr. 131*, 2491S−2497S.
(6) Gstraunthaler, G., Holcomb, T., Feifel, E., Liu, W., Spitaler, N., and Curthoys, N. P. (2000) Differential expression and acid-base regulation of glutaminase mRNAs in gluconeogenic LLC-PK(1)-FBPase(+) cells. *Am. J. Physiol. 278*, F227−F237.
(7) Chaudhry, F. A., Reimer, R. J., and Edwards, R. H. (2002) The glutamine commute: Take the N line and transfer to the A. *J. Cell Biol. 157*, 349−355.
(8) Hamberger, A., Chiang, G. H., Sandoval, E., and Cotman, C. W. (1979) Glutamate as a CNS transmitter. II. Regulation of synthesis in the releasable pool. *Brain Res. 168*, 531−541.
(9) Thanki, C. M., Sugden, D., Thomas, A. J., and Bradford, H. F. (1983) In vivo release from cerebral cortex of [^{14}C]glutamate synthesized from [U-^{14}C]glutamine. *J. Neurochem. 41*, 611−617.
(10) Masson, J., Darmon, M., Conjard, A., Chuhma, N., Ropert, N., Thoby-Brisson, M., Foutz, A. S., Parrot, S., Miller, G. M., Jorisch, R., Polan, J., Hamon, M., Hen, R., and Rayport, S. (2006) Mice lacking brain/kidney phosphate-activated glutaminase have impaired glutamatergic synaptic transmission, altered breathing, disorganized goal-directed behavior and die shortly after birth. *J. Neurosci. 26*, 4660−4671.
(11) Hoffman, E. M., Schechter, R., and Miller, K. E. (2010) Fixative composition alters distributions of immunoreactivity for glutaminase and two markers of nociceptive neurons, Nav1.8 and TRPV1, in the rat dorsal root ganglion. *J. Histochem. Cytochem. 58*, 329−344.
(12) Erdmann, N., Zhao, J., Lopez, A. L., Herek, S., Curthoys, N., Hexum, T. D., Tsukamoto, T., Ferraris, D., and Zheng, J. (2007) Glutamate production by HIV-1 infected human macrophage is blocked by the inhibition of glutaminase. *J. Neurochem. 102*, 539−549.
(13) Erdmann, N., Tian, C., Huang, Y., Zhao, J., Herek, S., Curthoys, N., and Zheng, J. (2009) In vitro glutaminase regulation and mechanisms of glutamate generation in HIV-1-infected macrophage. *J. Neurochem. 109*, 551−561.
(14) Elgadi, K. M., Meguid, R. A., Qian, M., Souba, W. W., and Abcouwer, S. F. (1999) Cloning and analysis of unique human glutaminase isoforms generated by tissue-specific alternative splicing. *Physiol. Genomics 1*, 51−62.
(15) Gao, P., Tchernyshyov, I., Chang, T. C., Lee, Y. S., Kita, K., Ochi, T., Zeller, K. I., De Marzo, A. M., Van Eyk, J. E., Mendell, J. T., and Dang, C. V. (2009) c-Myc suppression of miR-23a/b enhances mitochondrial glutaminase expression and glutamine metabolism. *Nature 458*, 762−765.
(16) Wang, J. B., Erickson, J. W., Fuji, R., Ramachandran, S., Gao, P., Dinavahi, R., Wilson, K. F., Ambrosio, A. L., Dias, S. M., Dang, C. V., and Cerione, R. A. (2010) Targeting mitochondrial glutaminase activity inhibits oncogenic transformation. *Cancer Cell 18*, 207−219.
(17) Robinson, M. M., McBryant, S. J., Tsukamoto, T., Rojas, C., Ferraris, D. V., Hamilton, S. K., Hansen, J. C., and Curthoys, N. P. (2007) Novel mechanism of inhibition of rat kidney-type glutaminase by bis-2-(5-phenylacetamido-1,2,4-thiadiazol-2-yl)ethyl sulfide (BPTES). *Biochem. J. 406*, 407−414.
(18) Otwinowski, Z., and Minor, W. (1997) Processing of X-ray Diffraction Data Collected in Oscillation Mode. *Methods Enzymol. 276*, 307−326.
(19) Collaborative Computational Project Number 4 (1994) The CCP4 suite: Programs for protein crystallography. *Acta Crystallogr. D50*, 760−763.
(20) Haddadian, E. J., Gong, H., Jha, A. K., Yang, X., DeBartolo, J., Hinshaw, J. R., Rice, P. A., Sosnick, T. R., and Freed, K. F. (2011) Automated Real-Space Refinement of Protein Structures Using a Realistic Backbone Move Set. *Biophys. J. 101*, 899−909.
(21) Laskowski, R. A., MacArthur, M. W., and Thornton, J. M. (1998) Validation of protein models derived from experiment. *Curr. Opin. Struct. Biol. 8*, 631−639.
(22) Segel, I. H. (1993) *Enzyme Kinetics: Behavior and Analysis of Rapid Equilibrium and Steady-State Enzyme Systems*, Wiley Classics Library, New York.
(23) Steckel, J., Roberts, J., Philips, F. S., and Chou, T. C. (1983) Kinetic properties and inhibition of *Acinetobacter* glutaminase-asparaginase. *Biochem. Pharmacol. 32*, 971−977.
(24) Brown, G., Singer, A., Proudfoot, M., Skarina, T., Kim, Y., Chang, C., Dementieva, I., Kuznetsova, E., Gonzalez, C. F., Joachimiak, A., Savchenko, A., and Yakunin, A. F. (2008) Functional and structural characterization of four glutaminases from *Escherichia coli* and *Bacillus subtilis*. *Biochemistry 47*, 5724−5735.